

Phenyl Derivative of Iron 5,10,15-Tritolylcorrole

Sara Nardis,[†] Daniel O. Cicero,[†] Silvia Licoccia,[†] Giuseppe Pomarico,[†] Beatrice Berionni Berna,[†] Marco Sette,[†] Giampaolo Ricciardi,[‡] Angela Rosa,^{*,‡} Frank R. Fronczeck,[§] Kevin M. Smith,^{*,§} and Roberto Paolesse^{*,†}

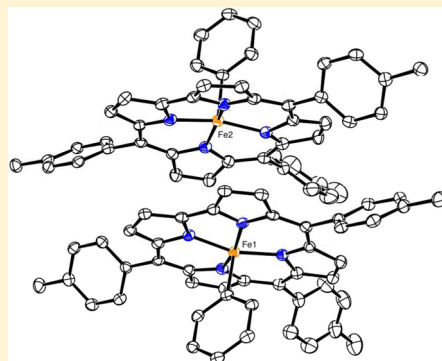
[†]Department of Chemical Science and Technologies, Università di Roma Tor Vergata, 00133 Roma, Italy

[‡]Dipartimento di Scienze, Università della Basilicata, 85100 Potenza, Italy

[§]Department of Chemistry, Louisiana State University, Baton Rouge, Louisiana 70803, United States

Supporting Information

ABSTRACT: The phenyl–iron complex of 5,10,15-tritolylcorrole was prepared by reaction of the starting chloro–iron complex with phenylmagnesium bromide in dichloromethane. The organometallic complex was fully characterized by a combination of spectroscopic methods, X-ray crystallography, and density functional theory (DFT) calculations. All of these techniques support the description of the electronic structure of this phenyl–iron derivative as a low-spin iron(IV) coordinated to a closed-shell corrolate trianion and to a phenyl monoanion. Complete assignments of the ¹H and ¹³C NMR spectra of the phenyl–iron derivative and the starting chloro–iron complex were performed on the basis of the NMR spectra of the regioselectively β -substituted bromo derivatives and the DFT calculations.



INTRODUCTION

Corrole was one of the first of the porphyrinoids to be reported in the literature,¹ having been prepared during the research wave that focused on the development of a synthetic route to vitamin B₁₂; it shares with corrin the molecular framework and with porphyrin the 18-electron π -aromatic system (Figure 1).²

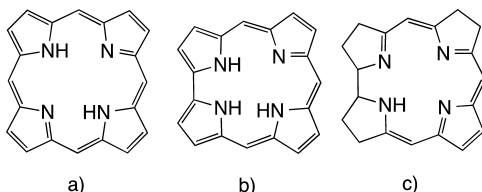


Figure 1. Molecular structure of porphyrin (a), corrole (b) and corrin (c).

The corrole macrocycle has recently received an impressive boost in published research,³ since it shows unusual properties that are different from those of the corresponding porphyrins but at the same time suggests promising practical applications.⁴ One of the corrole peculiarities is related to its coordinative behavior; being a trianionic ligand, corrole usually stabilizes coordinated metals in oxidation states formally higher than those of the corresponding porphyrin complexes. However, since corrole is also characterized by low oxidation potentials, a facile ligand-to-metal electron transfer can occur, introducing the so-called noninnocent character of the macrocycle as a ligand. This feature makes it quite difficult to establish the

electronic structures of corrole complexes, thereby making the characterization of its coordination chemistry both challenging and intriguing.

One of the most debated and interesting examples of the noninnocent ligand behavior is represented by iron-corrole derivatives.⁵ We reported the first iron–corrole complex, obtained as an Fe(III) derivative,⁶ and Vogel and co-workers later noticed that the air oxidation of such a species afforded the formally Fe(IV) complex, obtained as the μ -oxo species or as its monomeric chloro derivative, depending on the reaction workup.⁷ Reaction of this latter complex with pyridine afforded the corresponding Fe(III) bis(pyridino) derivative, where the axial coordination also induced a formal reduction of the metallic center.⁷

More recently, the development of synthetic routes for the preparation of 5,10,15-triarylcorroles has significantly widened the horizon of corrole chemistry and also the number of metal complexes,^{3c} presenting more opportunities to tune the ligand characteristics by synthetic modifications.^{3b} This beneficial expansion has also been useful for iron corrolates, and both spectroscopic and theoretical characterization of such complexes has further confirmed that chloro–iron corrole complexes are better described as Fe(III) [corrole]^{2•-}, where corrole is oxidized to a macrocyclic π -cation radical, according to its noninnocent character.⁵ We have recently exploited the π -cation radical nature of the complex for the preparation of β -

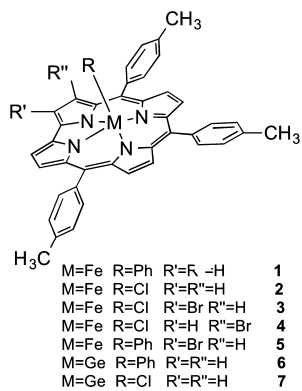
Received: February 13, 2014

Published: April 3, 2014

nitrocorrole iron complexes, obtained upon nucleophilic attack of the nitrite ion on the chloro–iron corrole complex.^{8,9}

On the other hand the μ -oxo dimer is better described as the Fe(IV) derivative, while the organometallic phenyl–iron β -alkylcorrole complexes^{5c} show more complex behavior: the NMR characterization, together with a density functional theory (DFT) study, show that the corrole assumes a total -3 charge, but the ligand noninnocence is still present, since appreciable radical character of the macrocycle has been reported.^{5c} The stabilization of the high oxidation state of the metal in the σ -phenyl iron–corrole complex has been explained based on the strong σ -donor nature of the phenyl axial ligand, which impedes ligand-to-metal electron transfer while not completely negating the radical character of the corrole. Although the σ -phenyl iron–corrole complex shows this peculiar behavior, it has been limited to the β -alkylcorrole derivatives⁷ and has not yet been reported for the triarylcorrole series.

For these reasons we have been interested in studying such a triarylcorrole species, and we now report the preparation and characterization of the phenyl–iron complex **1** of 5,10,15-tritylcorrole. Specifically, the X-ray structure, solution magnetic measurements, and ^1H and ^{13}C NMR spectra were acquired, and DFT calculations were performed. To obtain the complete assignment of the NMR spectra of **1**, the ^1H and ^{13}C NMR spectra of the ad hoc prepared β -substituted chloro–iron tritylcorrole complexes **3** and **4** and of the phenyl–iron derivative **5** were studied. For the sake of completeness the ^1H and ^{13}C NMR spectra of the chloro–iron derivative **2**, which is the precursor of **1**, were also investigated and assigned with the help of the spin-density pattern obtained by DFT calculations and the NMR spectra of the β -substituted derivatives **3** and **4**. To have a diamagnetic counterpart of the chloro– and phenyl–iron complexes, the germanium derivatives **6** and **7** were prepared and investigated by NMR spectroscopy.



EXPERIMENTAL SECTION

General. Reagents and solvents (Sigma-Aldrich, Fluka, and Carlo Erba Reagenti) for synthesis and purification were of synthetic grade and were used as received. NMR experiments were performed at $T = 300$ K on a Bruker Avance 600 MHz with a 5 mm inverse broadband probe equipped with z -axis gradients. All data were processed with TopSpin. Two-dimensional (2D) total correlation spectroscopy (TOCSY), nuclear Overhauser enhancement spectroscopy (NOESY), and ^1H – ^{13}C heteronuclear multiple-quantum correlation (HMQC) were recorded using standard pulse sequences. The Curie plot was obtained by acquiring the spectra over a temperature range from -53 to $+50$ °C. Ultraviolet-visible (UV-vis) spectra were measured in CH_2Cl_2 with a Varian Cary 50 spectrophotometer. Mass spectra (FAB mode) were recorded on a VGQuattro spectrometer in

the positive-ion mode using *m*-nitrobenzyl alcohol (Aldrich) as a matrix.

Magnetic Susceptibility Measurements. The magnetic susceptibility of compounds **1** and **2** was measured in CHCl_3 solution using NMR spectroscopy, following the method of Evans,¹⁰ using the equation of Sur for the geometry of a superconducting magnet,¹¹ and correcting for the diamagnetic contribution of the corrole ligand.¹² The results yielded a triplet ground state, consistent with magnetic data previously reported for several chloro– and phenyl–iron corrolates.^{5a,c,e,7,13}

Quantum Chemical Calculations. DFT geometry optimizations and ground-state electronic structure analyses were performed with the ADF (Amsterdam Density Functional) program system, release 2013.¹⁴ Two exchange-correlation functionals were employed: the recently implemented generalized gradient approximation (GGA) functional S12g,¹⁵ which includes Grimme's D3 dispersion energy^{16,17} and has been shown to yield correct spin-state relative stabilities for iron(II) complexes,¹⁵ and the hybrid B3LYP-D3 functional.^{16,18,19} The calculations were performed using the spin-unrestricted approach and included relativistic effects through the scalar zero-order regular approximation (ZORA) formalism.^{20–22} The all-electron ZORA/TZ2P basis set,²³ which is an uncontracted triple- ζ STO basis with two sets of polarization functions, was used for all atoms.

The ground-state geometries of compound **1** and **2** were optimized in vacuo without any symmetry constraint, assuming an $S = 1$ ground state, as indicated by magnetic susceptibility measurements. The optimized structures were verified to represent local minima by calculation of harmonic frequencies. Solvent effects on the ground-state properties were modeled through the conductor-like continuum solvent model (COSMO)^{24–26} using the same solvent employed in the NMR and magnetic susceptibility measurements. For the sake of comparison with previous results,^{5d,e} a natural orbital (NO) analysis was also performed for compound **2**. The NOs were computed with TURBOMOLE²⁷ through single-point calculations at the S12g and B3LYP ADF-optimized geometries. As in TURBOMOLE the S12g functional is not available, the pure GGA BP86 functional²⁸ was used instead. In the BP86 and B3LYP single-point calculations the def2-TZVP basis set,²⁹ which is an extensively polarized basis set of triple- ζ quality including high angular momentum polarization functions, was used. Solvent (CHCl_3) effects were modeled through the COSMO model.^{24,25} The NOs were visualized with gOpenMol.³⁰

Syntheses. 5,10,15-Tritolykorrole,³¹ 2-bromo-5,10,15-tritylkorrole, and 3-bromo-5,10,15-tritylkorrole,³² as well as the chloro–iron **2**³³ and chlorogermainium **7**³⁴ derivatives were prepared following literature methods.

Chloro-iron 2-bromo-5,10,15-tritylkorrole **3.** The title complex was prepared as reported for compound **2**, starting with 2-bromo-5,10,15-tritylkorrole. Yield: 75%. mp > 300 °C. UV-vis (dichloromethane): λ_{max} nm ($\log \epsilon$, $\text{M}^{-1} \text{cm}^{-1}$): 360 (4.66), 420 (4.62), 507 (4.15), 648 (3.05). Anal. Calcd for $\text{C}_{40}\text{H}_{28}\text{BrClFeN}_4$: C, 65.29; H 3.84; N, 7.61. Found: C, 65.31; H, 3.79; N 7.59%.

Chloro-iron 3-bromo-5,10,15-tritylkorrole **4.** The title complex was prepared as reported for compound **2**, starting with 3-bromo-5,10,15-tritylkorrole. Yield: 72%. mp > 300 °C. UV-vis (dichloromethane): λ_{max} nm ($\log \epsilon$, $\text{M}^{-1} \text{cm}^{-1}$): 363 (4.68), 418 (4.60), 508 (4.04), 650 (3.02). Anal. Calcd for $\text{C}_{40}\text{H}_{28}\text{BrClFeN}_4$: C, 65.29; H 3.84; N, 7.61. Found: C, 65.28; H 3.81; N, 7.63%.

Phenyl-Iron 5,10,15-Tritolykorrole **1.** The complex **2** (65 mg; 0.1 mmol) was dissolved in anhydrous dichloromethane (10 mL) and treated with 79 μL of a 3 M solution of phenylmagnesium bromide in diethyl ether. After 10 min water was added, the organic phase was separated and dried over anhydrous sodium sulfate, and the solvent was removed under vacuum. The reaction mixture was purified using a chromatographic column on silica gel, using dichloromethane/hexane (3:1) as eluent. The first red band was recrystallized from dichloromethane/methanol (2:1) to give red crystals of the title product. Yield: 70% (49 mg). mp > 300 °C. UV-vis (dichloromethane): λ_{max} nm ($\log \epsilon$, $\text{M}^{-1} \text{cm}^{-1}$): 382 (4.68), 504 (4.03), 554 (3.93), 651 (3.50). Anal. Calcd for $\text{C}_{46}\text{H}_{34}\text{FeN}_4$: C, 79.08; H, 4.91; N 8.02. Found: C, 79.05; H 4.94; N, 7.98%.

Scheme 1

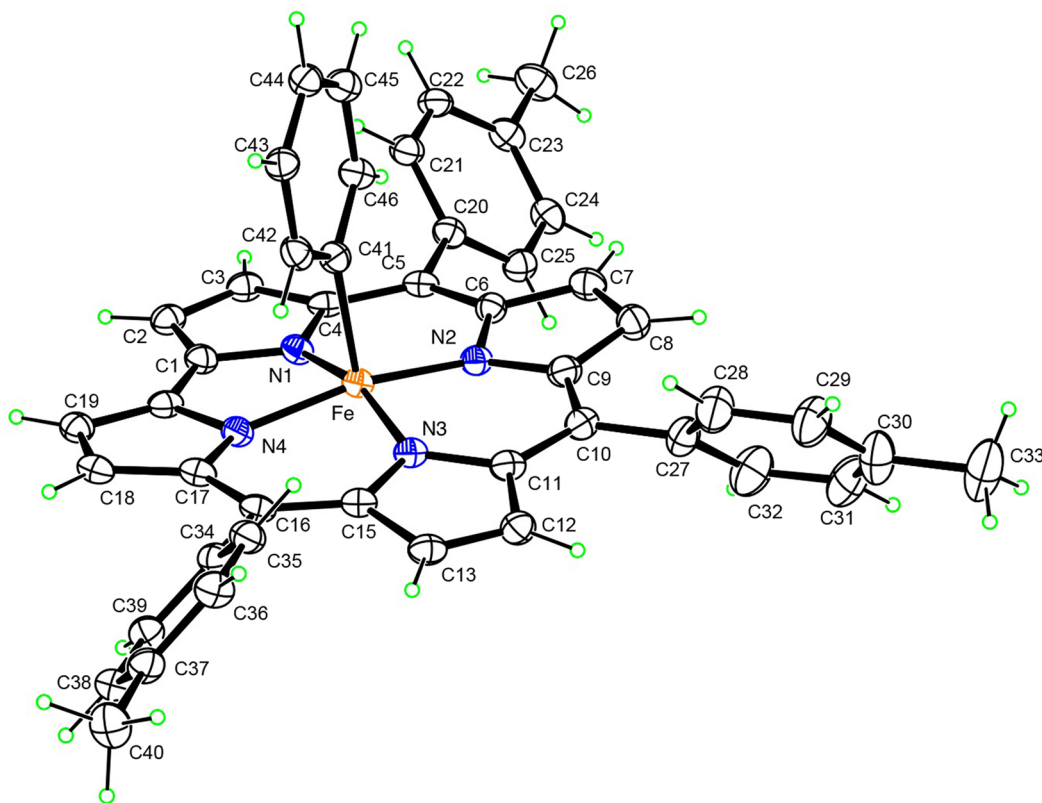
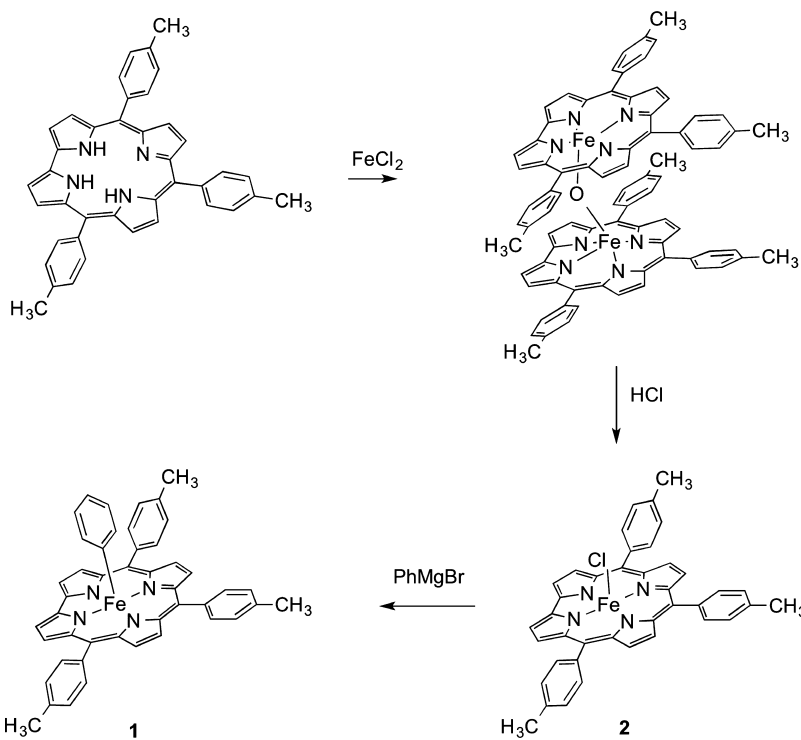


Figure 2. Molecular structure of 1.

X-ray. Crystallographic data were collected using $\text{Cu K}\alpha$ radiation ($\lambda = 1.54178 \text{ \AA}$) at $T = 90 \text{ K}$ on a Bruker Kappa APEX-II DUO diffractometer equipped with a $1\mu\text{s}$ microfocus source. Crystal data: $\text{C}_{46}\text{H}_{34}\text{FeN}_4$, (0.45 CH_2Cl_2), $M_r = 736.84$, monoclinic space group $P2_1/c$, $a = 13.5056(4)$, $b = 44.6178(14)$, $c = 13.2577(4) \text{ \AA}$, $\beta =$

$116.803(2)^\circ$, $V = 7130.6(4) \text{ \AA}^3$, $Z = 8$, $D_x = 1.373 \text{ Mg m}^{-3}$, $\theta_{\max} = 60.1^\circ$, $R = 0.057$ for 10 535 data (8121 with $I > 2\sigma(I)$) and 925 refined parameters. Disordered solvent contribution was removed from the data using the SQUEEZE procedure,³⁵ amounting to 0.45 dichloromethane molecules per corrole complex. CCDC 975295.

Phenyl-Iron 2-Bromo-5,10,15-tritolylcorrolate 5. The title complex was prepared as reported for compound **1**, starting from the chloro–iron derivative **3**. Yield: 71%. mp > 300 °C. UV-vis (dichloromethane): λ_{max} nm ($\log \epsilon$, M⁻¹ cm⁻¹): 384 (4.65), 507 (4.08), 547 (3.87), 648 (3.20). Anal. Calcd for C₄₆H₃₃BrFeN₄: C, 71.06; H, 4.28; N 7.21. Found: C, 70.98; H 4.25; N, 7.24%.

Phenyl-Germanium 5,10,15-Tritolylcorrolate 6. Chlorogermainium corrolate (100 mg; 0.15 mmol) was dissolved in anhydrous dichloromethane (15 mL) and treated with 119 μ L of a 3 M solution of phenylmagnesium bromide in diethyl ether. After 10 min water was added, the organic phase was separated, dried over anhydrous sodium sulfate, and then the solvent removed under vacuum. The crude mixture was filtered through a silica gel plug, using dichloromethane as eluent, and the collected band was crystallized from dichloromethane/methanol (2:1) to give crystals of the title product. Yield: 76% (81.5 mg). mp > 300 °C. UV-vis (CH₂Cl₂): λ_{max} nm ($\log \epsilon$, M⁻¹ cm⁻¹): 401 sh (4.53), 419 (5.18), 514 (3.68), 531 (3.77), 570 (3.91), 612 (4.44). Anal. Calcd for C₄₆H₃₄GeN₄: C, 77.23; H, 4.79; N 7.83. Found: C, 77.05; H 4.81; N, 7.80%.

RESULTS AND DISCUSSION

Synthesis and X-ray Characterization. The preparation of the corrole phenyl–iron derivative **1**, as indicated in Scheme 1, is quite straightforward, and follows the protocol already reported for the analogous β -octalkylcorrole complexes.⁷ The visible absorption spectrum of **1** is quite similar to those reported in the literature for related β -octalkylcorrole complexes, showing a Soret band at 382 nm and a broad Q band at 504 nm, with a shoulder at 554 nm. The FAB mass spectrum of **1** did not show the molecular ion, with a parent peak corresponding to the Fe–corrole residue, generated by the loss of the axial phenyl group under the ionization conditions. Complex **1** is air stable, and slow crystallization from methanol diffusion into a CHCl₃ solution of the iron derivative allowed formation of single crystals suitable for X-ray characterization.

The structure of compound **1** is shown in Figure 2. There are two independent molecules in the asymmetric unit, and both have very similar dimensions (Supporting Information, Figure S1). The Fe has a square pyramidal coordination geometry with Fe–N distances in the range of 1.858(3)–1.890(3) Å and Fe–C(phenyl) distances of 1.984(4) and 1.987(4) Å. The Fe atoms lie out of the corrole N₄ planes by 0.2524(6) and 0.2640(5) Å. The Fe–N bonds to the directly linked pyrroles, 1.858(3)–1.872(3), mean 1.864 Å, are slightly shorter than they are to the others, 1.884(3)–1.890(3), mean 1.888 Å. The 23-atom corrole cores of both independent molecules have nonplanar conformations, with small saddle distortions. For one molecule, the mean and maximum deviations from coplanarity are 0.077 and 0.199(3) Å, while for the other, these values are larger, 0.127 and 0.325(3) Å. The C_β atoms (C₂, C₃, C₇, C₈, etc.) are alternately above and below the best planes in pairs by average deviations of 0.128 and 0.251 Å, respectively, for the two molecules. The two molecules form a slipped, stacked dimer with Fe···Fe distance 5.153(1) Å. However, the two corrole planes are not parallel, forming a dihedral angle of 7.5(1)°. Closest intermolecular contacts are C···C 3.293(5) Å and Fe···C 3.517(4) Å.

It is of interest to compare the structure of **1** with those of octaethylcorrolato–phenyl–iron,⁷ (OEC)FePh, refcode SUMXED and its corresponding oxidized π cation radical [(OEC)FePh]ClO₄,³⁶ refcode ZOKCIL. Unlike the saddle corrole conformation of **1**, both of the octaethyl derivatives have more planar corroles (mean deviations of 0.037 Å for SUMXED and 0.022 Å for ZOKCIL), with almost all distal C

atoms on the side of the molecule opposite the coordinated phenyl group. In both octaethyl compounds, the Fe coordination is also square pyramidal, and as compared to **1**, the Fe out-of-plane distance is slightly larger: 0.272(1) Å for SUMXED and slightly smaller, 0.242(2) Å for ZOKCIL. The Fe–C(phenyl) distance in **1** agrees well with that in SUMXED, 1.984(7) Å, but it is slightly longer than that in the π cation radical, 1.965(5) Å. The Fe–N distances in **1** also agree well with those of SUMXED, but those of ZOKCIL are systematically smaller by an average value of 0.012 Å.

The same synthetic pathway adopted for the preparation of **1** was used to synthesize the Ge derivative **6**. This complex was prepared to provide a diamagnetic species analogous to the iron derivative and thereby to provide help for the NMR characterization of **1**.

DFT Calculations. Experimental and theoretical studies on β -substituted phenyl–iron corrolates have led to a consensus about the electronic structure of these complexes, namely, a low-spin iron(IV) that is coordinated to a closed-shell corrolate trianion and to a phenyl monoanion.^{5a,7,37–41} Our DFT-ZORA calculations on complex **1** support this view. A spin-coupled metal–radical system situation can be excluded on the basis of the computed $\langle S^2 \rangle$ value that was found to be very close to the value expected for a pure triplet state (2.05 and 2.10 at S12g and B3LYP-D3 level, respectively). Quite different is the situation for **2**. In agreement with previous experimental and theoretical studies,⁵ our DFT-ZORA calculations on complex **2** point to the existence of appreciable radical character of the corrole macrocycle. In this case the value computed for $\langle S^2 \rangle$ deviates significantly from that expected for a pure triplet state, particularly at B3LYP-D3 level. The calculated $\langle S^2 \rangle$ values are 2.37 and 2.76 at S12g and B3LYP-D3 level, respectively.

Molecular Structure. Table 1 lists selected structural parameters obtained for complex **1** from the S12g and B3LYP-D3 optimized geometries together with the X-ray structural data determined for the two independent molecules forming the crystalline asymmetric unit. The S12g optimized structure of **1** is shown in Figure 3. The two functionals yield rather similar geometries, save for the iron–phenyl distance, the displacement of the iron atom out of the (N_p)₄ and the 23-atom corrole planes, and the degree of tilting of the axial phenyl ligand with respect to the N₂–Fe–N₄ plane. Compared to S12g, B3LYP-D3 predicts a larger Fe–Ph distance and a less pronounced extrusion of the metal from both the (N_p)₄ and 23-atom corrole planes, in better agreement with the experiment. However, B3LYP-D3 largely underestimates the degree of tilting of the axial phenyl ligand with respect to the N₂–Fe–N₄ plane. Both, the S12g and B3LYP-D3 functionals reproduce the experimental Fe–N distances quite satisfactorily and account well for the occurrence of two short (Fe–N₁ and Fe–N₄) and two long (Fe–N₂ and Fe–N₃) Fe–N bonds in the complex. The calculations also account for the trend observed for the C_{meso}–C_{Tol} distances and the degree of tilting of the tolyl groups with respect to the 23-atom corrole plane. Indeed, both functionals predict a lengthening of the C₁₀–C_{Tol} bond relative to the C₅–C_{Tol} and C₁₅–C_{Tol} bonds, and a less pronounced tilting of the tolyl group bound to C₁₀, both features reflecting somewhat less effective conjugation between this tolyl group and the corrole π system.⁴²

As for the chloro–iron complex, the relevant structural parameters obtained from the S12g and B3LYP-D3 optimized geometries are gathered in Table 2 and are compared to the X-ray data available for the chloro–iron corrolate analogue, the

Table 1. Selected Bond Lengths (Å), Dihedral Angles (deg), and Metrical Parameters(Å) Calculated for Complex 1

	DFT-ZORA		exp ^a	
	S12g	B3LYP-D3	A	B
Fe–N ₁	1.872	1.864	1.858(3)	1.860(3)
Fe–N ₂	1.899	1.899	1.883(3)	1.884(3)
Fe–N ₃	1.896	1.889	1.890(3)	1.890(3)
Fe–N ₄	1.871	1.876	1.867(3)	1.872(3)
Fe–Ph	1.954	1.973	1.987(4)	1.984(4)
C ₅ –C _{Tol}	1.480	1.484	1.487(5)	1.481(5)
C ₁₀ –C _{Tol}	1.485	1.488	1.490(6)	1.486(6)
C ₁₅ –C _{Tol}	1.482	1.482	1.486(5)	1.479(5)
θ ₁ ^b	67.3	57.4	48.88(7)	41.36(7)
θ ₂ ^c	74.8	63.6	51.28(11)	46.78(13)
θ ₃ ^d	63.7	60.3	46.40(11)	44.65(11)
θ ₄ ^e	45.5	35.0	46.9(3)	52.6(4)
ΔFe ^f	0.328	0.279	0.2521(15)	0.2485(9)
ΔFe ^g	0.451	0.198	0.2639(16)	0.2864(9)

^aExperimental values for **1** (this work); A and B refer to the two independent molecules in the crystal. ^bDihedral angle between the plane of the tolyl group bound to the meso C₅ atom and the 23-atom corrole plane. ^cDihedral angle between the plane of the tolyl group bound to the meso C₁₀ atom and the 23-atom corrole plane. ^dDihedral angle between the plane of the tolyl group bound to the meso C₁₅ atom and the 23-atom corrole plane. ^eDihedral angle between the phenyl plane and the plane passing through N₂–Fe–N₄. ^fDisplacement of the Fe atom out of the (N_p)₄ plane. ^gDisplacement of the Fe atom out of the 23-atom corrole plane.

TPFCorrFeCl complex.⁴³ Just as in the case of the phenyl–iron complex, S12g and B3LYP-D3 calculations yield rather similar geometries, except for the Fe–Cl distance that at B3LYP-D3 level is predicted to be ca. 0.04 Å longer than at S12g level. What we find is in line with previous DFT calculations on axially ligated iron corroles, which indicate that B3LYP tends to predict larger iron–ligand distances compared to pure GGA functionals such as BP86.^{5f} While the Fe–N distances and the displacement of the iron atom out of the (N_p)₄ and the 23-atom corrole planes match well with the experiment, the Fe–Cl distance is somewhat underestimated, particularly at S12g level.

Electronic Structure and Spin Densities. Figure 4 shows a molecular orbital (MO) diagram of complex **1** obtained at the S12g level of theory. A similar MO pattern was obtained using the B3LYP-D3 functional. In the complex, the phenyl–iron(IV) ($S = 1$) moiety is, just as the oxoiron(IV) ($S = 1$) moiety is in oxoiron(IV) porphyrin complexes,⁴⁴ a d⁴ system with a (d_{xy})²(d_{xz})¹(d_{yz})¹ electronic configuration. The Fe–Ph bond is formed by a σ interaction between the (nominally unoccupied) Fe 3d_{z²} orbital and the highest occupied (HOMO) of the Ph[−] fragment having large amplitude on the C1–2p_z orbital (cf. the σ and σ^* MOs in Figure 4), and a π interaction between the (nominally half occupied) Fe 3d_{xz,yz} orbitals and the occupied π MOs of the Ph[−] fragment, mainly the HOMO–1 and HOMO–4. In Figure 4 only the Fe–Ph π -antibonding MOs (which are nominally the d _{π} orbitals and are denoted as π_{xz} and π_{yz}) are reported. Of the Fe d _{δ} orbitals, the fully occupied d_{xy} is substantially a nonbonding orbital, whereas the empty d_{x²–y²}, with lobes along the axes, is destabilized by antibonding interaction with the σ lone pairs of the equatorial nitrogens. This MO, denoted as σ'^* , ends up above the corrole “e_g*-like” MOs (the β -spin component of the σ'^* is too high in energy to enter the diagram of Figure 4).

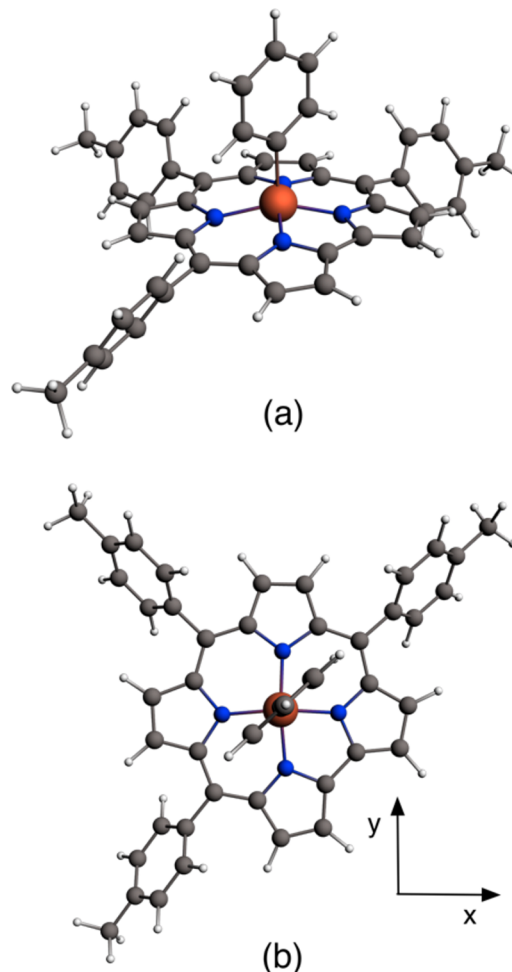


Figure 3. Top view (a) and side view (b) of the molecular structure of **1** optimized at DFT-ZORA/S12g/TZ2P level of theory, in vacuo.

Table 2. Selected Bond Lengths (Å), Dihedral Angles (deg), and Metrical Parameters (Å) Calculated for Complex 2

	DFT-ZORA		
	S12g	B3LYP-D3	exp ^a
Fe–N ₁	1.892	1.900	1.882(7)
Fe–N ₂	1.927	1.938	1.919(6)
Fe–N ₃	1.919	1.929	1.922(7)
Fe–N ₄	1.896	1.905	1.880(6)
Fe–Cl	2.177	2.219	2.238
C ₅ –C _{Tol}	1.478	1.479	
C ₁₀ –C _{Tol}	1.489	1.484	
C ₁₅ –C _{Tol}	1.479	1.480	
θ ₁ ^b	56.2	61.4	
θ ₂ ^c	60.7	67.9	
θ ₃ ^d	57.2	62.7	
ΔFe ^e	0.423	0.428	0.3670(11)
ΔFe ^f	0.510	0.512	0.4034(11)

^aExperimental values for TPFCorrFeCl, from reference 43. ^bDihedral angle between the plane of the tolyl group bound to the meso C₅ atom and the 23-atom corrole plane. ^cDihedral angle between the plane of the tolyl group bound to the meso C₁₀ atom and the 23-atom corrole plane. ^dDihedral angle between the plane of the tolyl group bound to the meso C₁₅ atom and the 23-atom corrole plane. ^eDisplacement of the Fe atom out of the (N_p)₄ plane. ^fDisplacement of the Fe atom out of the 23-atom corrole plane.

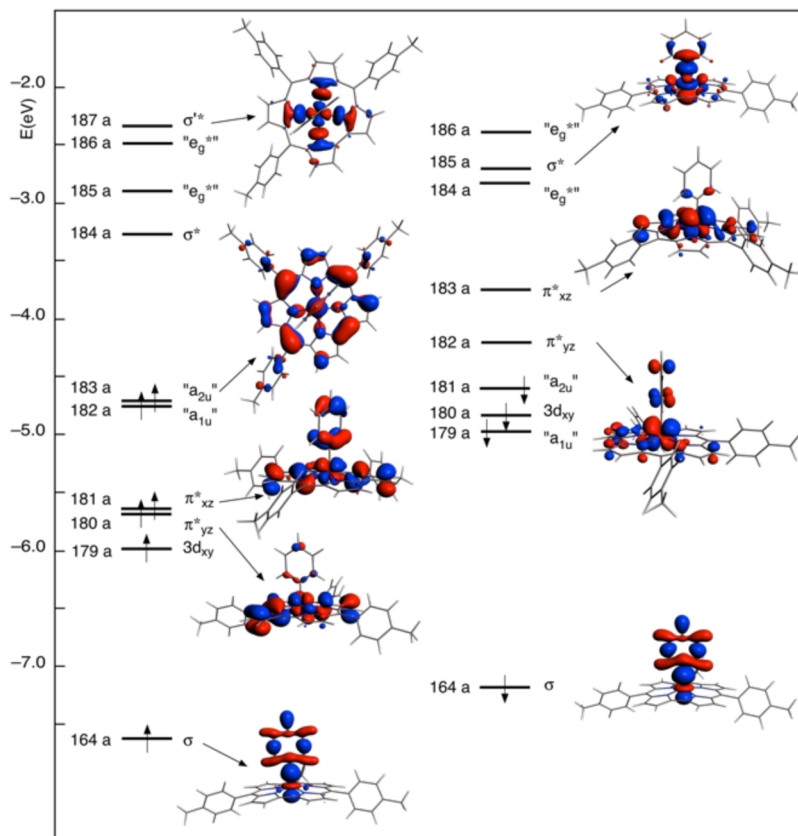


Figure 4. Diagram of selected energy levels and relevant molecular orbitals of complex **1** in the $S = 1$ spin state obtained from DFT-ZORA/S12g/COSMO/TZ2P calculations, in CHCl_3 solution.

Table 3. Mulliken Gross Population of Iron 3d Orbitals Computed for Complexes **1 and **2** in CHCl_3 Solution**

orbital ^a	1				2			
	S12g		B3LYP-D3		S12g		B3LYP-D3	
	spin α	spin β						
$3d_{z^2}$	0.68	0.52	0.74	0.51	0.83	0.35	0.95	0.29
$3d_{x^2-y^2}$	0.48	0.40	0.47	0.37	0.49	0.38	0.46	0.34
$3d_{xy}$	0.96	0.94	0.98	0.96	0.97	0.94	0.98	0.96
$3d_{xz}$	0.98	0.23	0.99	0.15	0.98	0.21	1.00	0.16
$3d_{yz}$	0.98	0.24	0.99	0.16	0.98	0.21	1.00	0.16

^aSummation over all MOs, multiplied by occupations.

The nature of the above-described bonding interactions is substantiated by the Mulliken gross population of the Fe 3d orbitals reported in Table 3. It is clear from the data in the Table that both spin components of the $3d_{xy}$ and the α spin component of the $3d_{xz}$ and $3d_{yz}$ are fully occupied, in agreement with a formal low spin d^4 electron configuration of the iron.

The β spin component of the $3d_{\pi}$ orbitals shows the charge accumulating as a consequence of the π donation by the axial phenyl ligand. According to the gross population of the 3d orbitals in Table 3, ca. 0.9 electrons are distributed over the two spin components of the Fe $3d_{x^2-y^2}$, owing to its participation in the low-lying Fe–N_{lp} (lp = lone pair) MOs, although one classifies these as “ligand” (N_{lp}) orbitals. The empty α and β spin σ'^* MOs are nominally the “ $3d_{x^2-y^2}$ ” but are certainly not pure metal orbitals, having no less than 40% of ligand (N_{lp}) character. The considerable population of the α and β spin components of the $3d_{z^2}$ orbital arises mainly from the

participation of this orbital in the occupied Fe–Ph σ MOs (see the plots of these orbitals in Figure 5) and, to a lesser extent, from donation by the “ a_{2u} -like” corrole orbital. Dissimilar from the a_{1u} -like MOs, the two components of the a_{2u} -like orbitals, especially the α spin component, are in fact not pure ligand orbitals. They have some (5–7%) Fe $3d_{z^2}$ character, as is evident from the plot of the α spin a_{2u} -like MO in Figure 5. This interaction, which is enabled by the displacement of the iron atom out of the corrole plane, induces a little spin polarization of the a_{2u} -like orbital. This explains why the spin density distribution in the tritylcorrole moiety largely reflects the atomic orbital composition of the a_{2u} -like MO. As a matter of fact the nitrogen and *meso*-carbon atoms carry a (small) negative spin density, while the C _{α} atoms of the pyrroles to which they are attached show smaller positive spin densities, except for the C _{α} atoms bound to C10 that, at S12g level, have negative spin density. All C _{β} atoms have positive spin densities, with values larger at S12g than at B3LYP-D3 level. Small spin

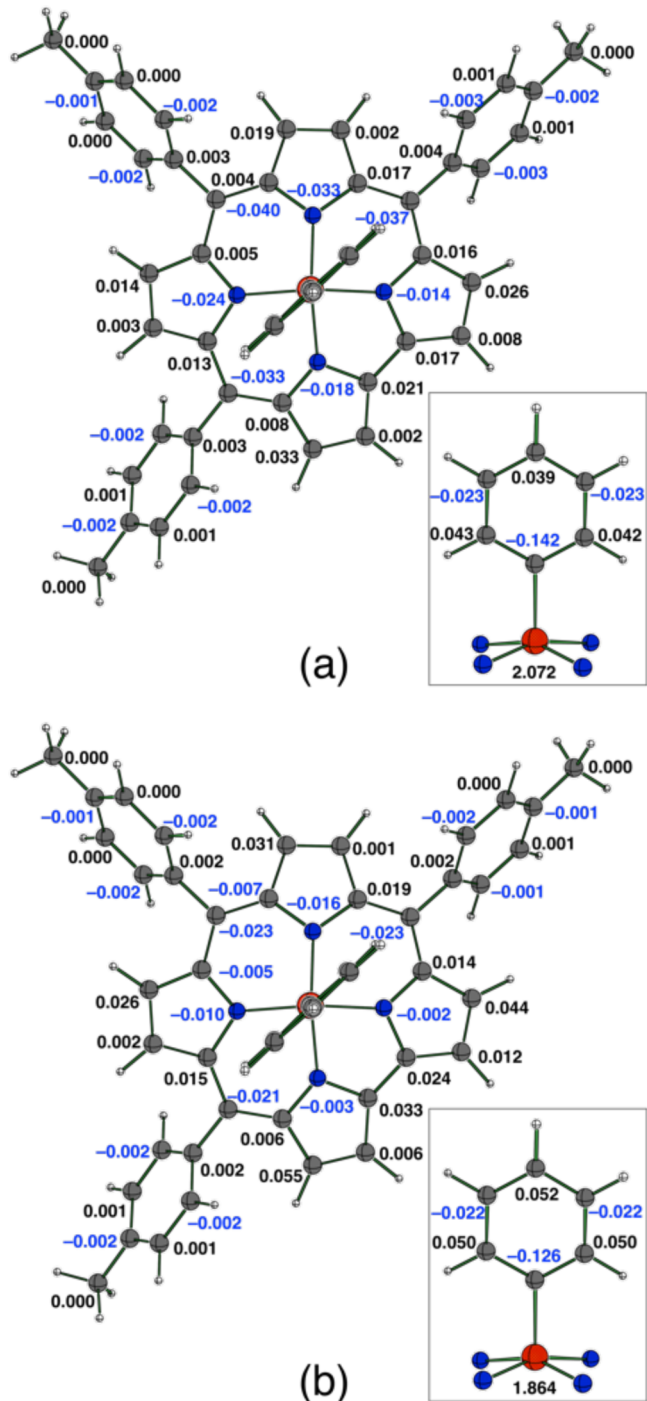


Figure 5. Atomic spin density distribution for complex **1** in the $S = 1$ spin state obtained from DFT-ZORA/COSMO/TZ2P calculations in CHCl_3 solution using B3LYP-D3 (a) and S12g (b) functionals.

densities with alternating signs on adjacent atoms are also found on the carbon atoms of the tolyl groups, on account of the a_{2u} -like MO having some amplitude also on the o - and p -carbons of the tolyl groups (see the plot of the α spin component of the a_{2u} -like MO in Figure 5).

The spin density on the metal is typical for Fe(IV) $S = 1$ and arises mainly from the $3d_{xz}$ and $3d_{yz}$ contributions. Compared to B3LYP-D3, S12g gives a smaller spin density on the metal (1.864 vs 2.072). This is in line with the well-known tendency of GGA functionals to overestimate metal–ligand covalency.^{5e}

The m -, o -, and p -carbon atoms of the axial phenyl ligand carry appreciable spin densities with alternating signs, the spin density on the carbanion C1 amounting to -0.142 and -0.126 at B3LYP-D3 and S12g level, respectively.

As discussed in the NMR section, the comparison between the measured isotropic shifts and the computed spin densities is overall quite satisfactory. The atomic spin densities obtained with the pure S12g functional better account, however, for the isotropic shifts measured for the C_β and tolyl protons.

The MO diagram of the chloro–iron derivative obtained at the S12g level of theory is shown in Figure 6. As in the phenyl–iron complex, the bond with the axial ligand consists of a σ interaction between the (nominally unoccupied) Fe $3d_{z^2}$ orbital and the Cl $3p_z$ orbital (cf. the σ and σ^* MOs in Figure 6) and a π interaction between the (nominally half occupied) Fe $3d_{x^2-y^2}$ orbitals and the occupied Cl $3p_{x,y}$. The metal–corrole bond interaction is significantly different in the two complexes, however. According to the orbital diagram of Figure 6, in the spin-up manifold the corrole a_{2u} -like MO mixes to some extent with the Fe $3d_{z^2}/\text{Cl } 3p_z$ σ -antibonding orbital (σ^*). Of the resulting occupied 170a and the empty 172a MOs, the former has a dominant σ^* character, while the latter is largely the corrole a_{2u} -like orbital (see the plots of these MOs in Figure 6). In the spin-down manifold the corrole a_{2u} -like MO remains, instead, an almost pure ligand orbital. The mixing between the corrole a_{2u} -like MO and the σ^* occurring in the spin-up manifold reflects on the Mulliken gross population of the α spin component of the Fe $3d_{z^2}$ orbital that is in the chloro–iron complex larger than it is in the phenyl–iron analog (Table 3) in spite of the lower σ donor capability of the axial ligand in **2** (note in Table 3 the diminished population of the β spin Fe $3d_{z^2}$ when moving from **1** to **2**). The population of the α spin component of the Fe $3d_{z^2}$ orbital is particularly large at B3LYP-D3 level as an indication of a more effective charge transfer from the corrole a_{2u} -like MO into the Fe $3d_{z^2}$ and hence of a more pronounced radical character of the corrole macrocycle. Anyway, both the pure and hybrid functionals agree on that, at variance with the phenyl–iron analog, the chloro–iron complex does not feature a closed-shell corrolate trianion. This does not mean, however, that in complex **2** an entire electron has been transferred from the corrolate trianion into the formally empty σ^* , turning the $[\text{Fe}^{\text{IV}}(\text{corrolate}^{3-})]\text{Cl}$ system into a $[\text{Fe}^{\text{III}}(\text{corrolate}^{2-})]\text{Cl}$ diradical and the corrole into a non-innocent ligand. In fact, the electron donation from the corrolate trianion into the σ^* may be accomplished not only through antiferromagnetic exchange coupling between the unpaired spins residing on (weakly) overlapping orbitals but also through a covalent interaction. To assess the noninnocence of the corrole macrocycle one should be able to distinguish between covalent and diradical character contributions to the ground-state wave function. Pierloot et al.^{5f} have recently suggested a procedure to evaluate the diradical character of a bond based on the natural orbital occupation numbers (NOON) involved in the bond. This procedure has been applied by these authors to provide a quantitative estimate of the diradical character of the metal–corrole bond in some copper and iron corroles. In particular, using the NOON of the bonding and antibonding combinations of the Fe $3d_{z^2}$ and the corrole a_{2u} -like MOs previously computed for unsubstituted chloro–iron corrole by Roos, Ghosh, and co-workers at CASSCF level,^{5e} Pierloot et al.^{5f} predicted for this complex a diradical character of only 59%. For the sake of comparison with these results, we applied the procedure suggested by

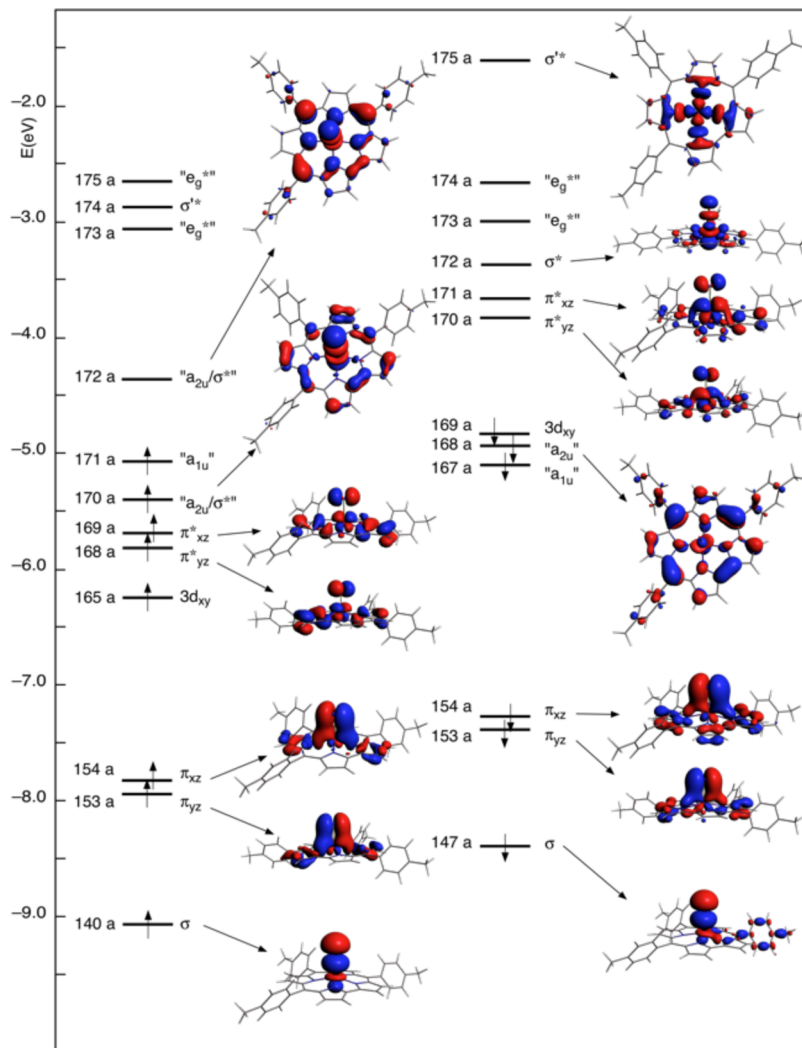


Figure 6. Diagram of selected energy levels and relevant molecular orbitals of complex **2** in the $S = 1$ spin state obtained from DFT-ZORA/S12g/COSMO/TZ2P calculations, in CHCl_3 solution.

Pierloot et al. to the chloro–iron complex here investigated. To this end we performed for complex **2** a NO analysis, both at B3LYP and at BP86 levels. The calculations showed the occurrence of two NO with occupation numbers that strongly deviate from either 2 or zero, the 169a and 172a, with occupations of 1.48 and 0.52 at B3LYP level, 1.84 and 0.16 at BP86 level. As can be inferred from the plots of the 169a and 172a in Figure 7, these NOs are the bonding and antibonding combination of the corrole a_{2u} -like MO and the σ^* . The diradical character of **2** obtained from the B3LYP NOON amounts to 52%, while that obtained from the BP86 NOON is only 16%, a value that is significantly smaller than that predicted for the unsubstituted chloro–iron complex using CASSCF natural orbitals. As it is presumable that the diradical character obtained from the S12g NOON would not be much different from that obtained from the BP86 NOON, is not surprising that the spin density pattern obtained at B3LYP-D3 level is quite different from that obtained at S12g level (Figure 8). Both functionals predict large negative spin densities at the meso positions, larger than in complex **1**. However, the B3LYP-D3 spin densities are significantly more negative than the S12g ones, which is consistent with the more pronounced diradical character predicted for complex **2** by the hybrid functional. On

account of the enhanced correlo-to-metal charge transfer in the chloro–iron complex the metal carries a larger spin density than in the phenyl–iron analog, particularly at the B3LYP-D3 level, in which case the spin density approaches that of a ferric iron of intermediate spin.

NMR Characterization. The ^1H NMR characterization of phenyl–iron derivatives of corrole has been reported for β -alkylcorroles,³⁷ while only the analogous phenyl–iron(IV) *meso*-arylporphyrin complexes can be found in the literature.⁴⁵ Figure 9a shows the ^1H NMR spectrum of complex **1**. Two distinct signals are observed for both the *o*- and *m*-protons of the tolyl substituents of the two compounds. This is due to a relatively high rotational barrier that causes the appearance of two separated signals for protons pointing in the two different directions with respect to the plane of the macrocycle. Assignment of the tolyl resonances was possible using a combination of TOCSY and NOESY spectra. Resonances belonging to the axial Phe ligand were assigned by comparison with data already available for similar compounds.³⁷ In particular, the *p*-proton of the Phe ligand was readily assigned, being the only proton showing an integral equal to 1. The spectrum of complex **1** shows large isotropic shifts for the axial Phe ligand and three β -pyrrolic protons (positions 2/18, 7/13

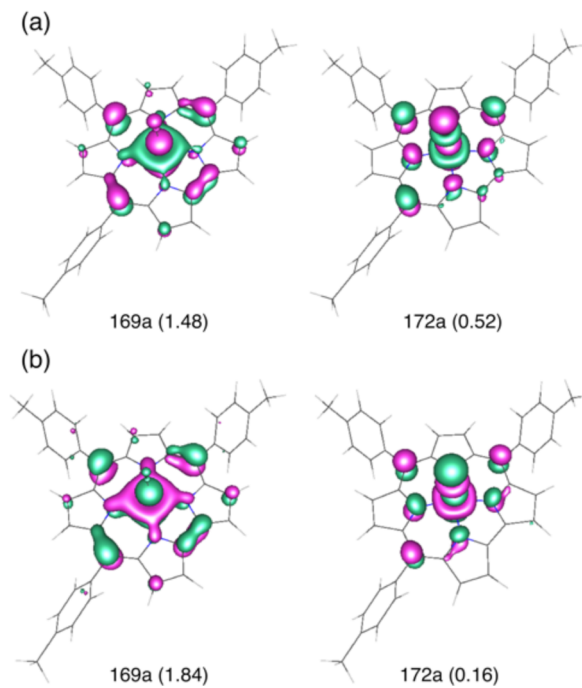


Figure 7. Natural orbitals and their occupation numbers (in parentheses) involved in the interaction between the σ^* and the corrole a_{2u} -like orbitals obtained for complex **2** from unrestricted B3LYP (a) and BP86 (b) calculations. The contour values are $\pm 0.04 \text{ e/au}^3$.

and 8/12), which ended in the -40 to -160 ppm spectral region. Smaller isotropic shifts were observed for the tolyl protons. No cross peak was detected for the β -pyrrolic protons in COSY and NOESY spectra, precluding an unambiguous assignment of these signals. To overcome this problem, it was decided to prepare the phenyl–iron derivatives of the monosubstituted complex **5**, taking advantage of the regioselectivity showed by corrole in the substitution reactions. The free base 2-bromo-5,10,15-tritolylcorrole, together with the corresponding 3-Br regioisomer, was prepared in satisfying yields as previously reported;³² other than having the possibility of obtaining both regioisomers, the choice of the Br substituents was designed to minimize the impact of the β substituents on the electronic characteristics of the corresponding iron complexes. The introduction of the Br atom at the 2 position renders the 3,17 protons nonequivalent, and consequently the signal was split into two, with the concomitant reduction of the intensity of the signal related to the residual 18 proton (Figure 9b). In Supporting Information, Figure S2 are shown the chemical shifts of the protons of complex **1** as a function of $1/T$. All resonances extrapolate to the diamagnetic region of the NMR spectrum, suggesting that the spin state of complex **1** is pure, with no thermally accessible excited state available. The magnetic moment of **1** was determined using the Evans method; the value obtained was $3.0 \mu_B$, consistent with a triplet ground state.

Figure 10a shows the ^1H NMR spectrum of the chloro–iron complex **2**. The unambiguous assignment of the β -pyrrolic proton resonances is not possible, since also in this case no cross peak was detected for these signals in COSY and NOESY spectra, due to their short relaxation times. In the literature this assignment has been achieved on the basis of DFT calculations^{5b,13} or by regioselective partial deuteration.⁴⁶ The

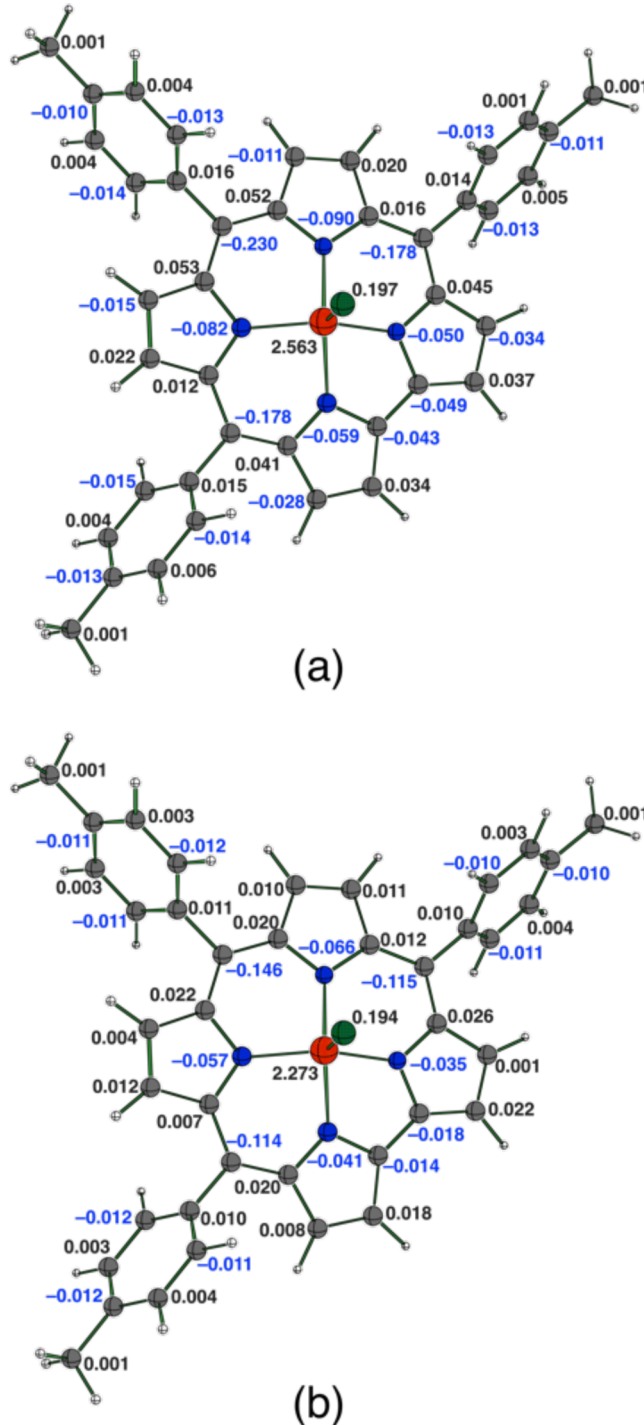


Figure 8. Atomic spin density distribution for complex **2** in the $S = 1$ spin state obtained from DFT-ZORA/COSMO/TZ2P calculations in CHCl_3 solution using B3LYP-D3 (a) and S12g (b) functionals.

substituted complexes **3** (with a bromine in position 2) and **4** (bromine in position 3) gave us the opportunity to perform the complete assignment of the ^1H NMR spectrum of complex **2** by selective substitution, as was done in the past for the complete assignments of the resonances of the analogous β -alkyl corrole complexes.^{5a} While in the spectrum of complex **3** it is possible to observe the reduction of intensity of the signal around -40 ppm, in the spectrum of compound **4** in this region it is possible to observe two resonances due to the presence of the Br in position 3, which makes the 2,18 protons

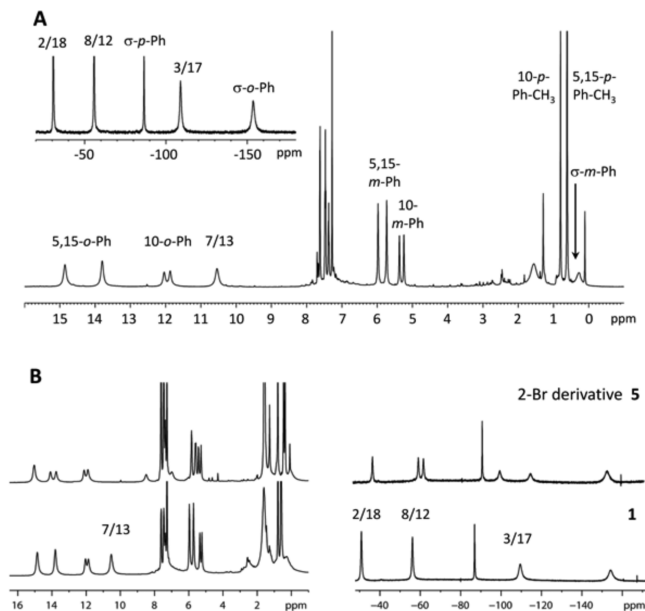


Figure 9. 1D ^1H NMR spectrum in CDCl_3 at 300 K of complex **1** (a) and comparison with the spectrum of the 2-Br derivative **5** (b).

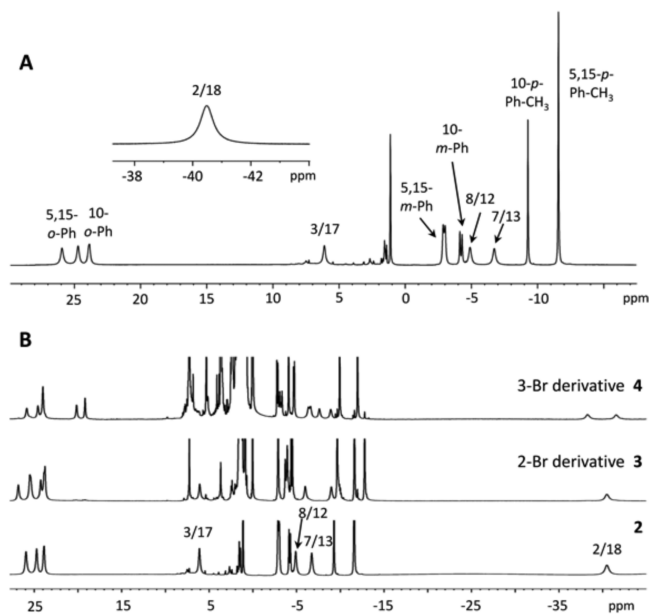


Figure 10. 1D ^1H NMR spectrum in CDCl_3 at 300 K of **2** (a) and the comparison with the corresponding spectra of the substituted complexes **3** and **4** (b).

no more equivalent (Figure 10b). These results consequently assign the high-field resonance to the 2,18 protons and not to the 3,17 analogous, as previously reported.

Table 4 shows the values for the measured ^1H isotropic shifts for all the protons in compounds **1** and **2**. Isotropic shifts were calculated using the corresponding Ge complexes as reference, and the estimated contact shifts were derived using an approximate value for the dipolar contribution.²³ It is interesting to note that the spin densities obtained by DFT/S12g calculations nicely support the assignments of the chemical shifts for complexes **1** and **2**, as reported in Table 4, and they better account for the isotropic shifts measured for the C_β and tolyl protons than do the spin densities calculated

Table 4. ^1H Chemical Shifts of Complexes **1** and **2** in CDCl_3 at 300 K

	chemical shift ppm	isotropic shift ^a ppm	contact shift ^b ppm	C spin density ^c	
1					
14.8, 13.8	6.6, 5.7	+3.3, +2.7	25.9, 24.7	17.6, 16.4	+14.6, +13.4
12.0, 11.9	3.9, 3.9	+0.9, +0.9	23.9, 23.8	15.8, 15.8	+12.8, +12.8
6.0, 5.7	-1.6, -1.9	-2.6, -2.9	-2.9, -3.0	-10.6, -10.7	-11.6, -11.7
5.4, 5.2	-2.2, -2.4	-3.2, -3.4	-4.1, -4.3	-11.7, -12.0	-12.7, -13.0
0.8	-1.9	-1.9	-11.6	-14.3	-14.3
0.6	-2.1	-2.1	+0.000	-9.3	-12.1
-30.7	-40.1	-43.9	+0.005	-49.9	-53.7
-109.1	-118.5	-122.3	+0.030	6.1	-3.0
10.5	1.3	-2.5	+0.002	-6.7	-16.0
-55.9	-64.7	-68.5	+0.017	-4.9	-13.9
-154.0	-156.3	-137.6	+0.042	+4.8	-17.7
0.3	-5.4	-4.8	-0.023	-6.8	-19.8
	-86.7	-92.7		-83.8	+0.007
				-83.8	+0.004
				-7/13-H ^d	+0.011
				8/12-H ^d	+0.003
				σ-o-Ph-H	+0.001
				σ-m-Ph-H	+0.002
				σ-p-Ph-H	+0.003
				σ-m-Ph-H	+0.003
				σ-p-Ph-H	+0.004
				σ-p-Ph-H	+0.005

^aIsotropic shift = observed chemical shift – diamagnetic shift. ^bEstimated using dipolar shifts calculated in reference 23 for a similar compound. ^cCarbon spin density obtained from DFT/S12g calculations, this work. ^dAssignments based on the relative spin densities and the observed chemical shifts of the 2- and 3-bromo derivatives.

by DFT/B3LYP-D3. In the case of complex **2**, for example, the C_{β} protons did not show an alternating sign in the isotropic shifts, expected from the spin density obtained calculated by DFT/B3LYP-D3, in accord with the pattern obtained by DFT/S12g calculations. NMR data show an alternating sign in the isotropic shift for *o*- and *m*-positions of the tolyl substituents, the shift for the *o*-protons being larger than that of the *m*-protons. This observation is in agreement with DFT/S12g calculations showing alternating signs for the spin density at these two positions. This is consistent with the presence of negative spin density at the meso carbons, although the effect is much smaller than it is in complex **2**, as suggested by the smaller observed isotropic shifts of *meso*-phenyl protons of complex **1** compared to **2**, and the relatively low calculated spin densities ($\Sigma|\rho_{\text{meso}}| = 0.07$ for complex **1**). On the other hand, DFT/S12g calculations predict spin densities at the β carbons larger for complex **1** ($\Sigma|\rho_{\text{pyrrole}}| \approx 0.18$) than for **2** ($\Sigma|\rho_{\text{pyrrole}}| \approx 0.09$), which is consistent with the relatively large isotropic shifts observed for the β -pyrrolic protons of **1**.

The chemical shifts for ^{13}C nuclei with favorable relaxation rates were measured using the 2D HMQC correlation experiment. Attempts to observe the remaining ^{13}C nuclei using one-dimensional (1D) experiment failed. Figure 11 shows

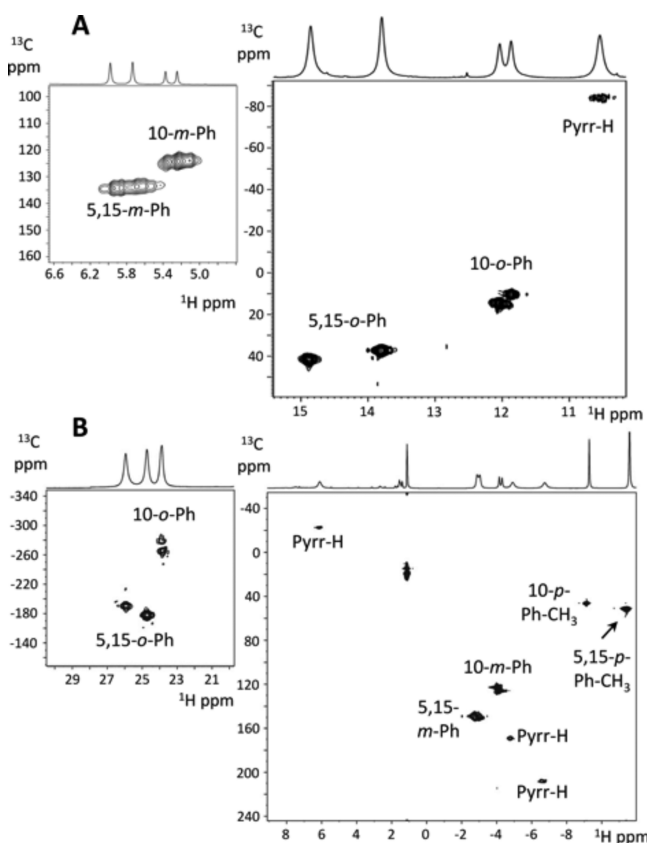


Figure 11. Selected regions of the 2D ^1H - ^{13}C HMQC correlation spectra of complexes **1** (a) and **2** (b).

selected regions of these experiments for complexes **1** and **2**. Table 5 shows the observed chemical shifts and the calculated isotropic shifts using the corresponding Ge complexes as the source of the diamagnetic shifts. In general, the ^{13}C isotropic shifts show the same trend as those of ^1H , reflecting the differences already discussed between the two compounds. ^{13}C shifts carry additional information about the pattern of spin

density and are more readily converted into quantitative estimation.^{5b} The two sources contributing to the ^{13}C paramagnetic shifts are those of dipolar nature and the contact contribution due to spin delocalization. The first, in the case of ^{13}C , is divided into two contributions: the metal- and the ligand-centered pseudocontact shifts. Compared to the large isotropic shifts normally observed for ^{13}C , their values are relatively small,^{47–49} accounting for about 10% of the total paramagnetic shift. For this reason, one can draw conclusions based on the second source, which in turn has two different contributions: the delocalization of metal electrons to the macrocycle through Corr \rightarrow Fe π donation, and the residual due to the corrole π radical electron. For meso substituents, however, only the latter is important for determination of the ^{13}C isotropic shifts, because the corrolate orbitals with which the metal d_{π} orbitals interact to delocalize the spin to the macrocyclic ring have nodes at the meso positions.^{5c}

In fact, it was calculated that for one or two delocalized electrons, the contribution to the *o*- and *m*-position of *meso*-phenyl substituent carbons accounts only for -3 to -6 ppm, respectively, of the total anisotropic shift.^{5c} So the large isotropic shifts observed for the *o*-carbons (in the range of -100 to -400 ppm), both for complexes **1** and **2** (see Table 5), are clear evidence of the presence of a negative spin density at the *meso*-carbons. Isotropic shifts of the *o*-carbons of the tolyl substituents are about 4 times larger for complex **2** than they are for **1**, reflecting the higher noninnocent character of the corrole ligand in **2**.

Peculiar behavior is observed for the sign of the isotropic shift of *m*-carbons in the two compounds. Those in positions 5,15 show positive isotropic shifts, as expected, due to the alternation in sign between the *o*- and *m*-positions. However, the tolyl substituent in position 10 shows small negative isotropic shifts. Since the expected contribution to the isotropic shift arising from the delocalization of metal electrons to the macrocycle is in the order of -3 ppm (one electron) or -5 ppm (two electrons),^{5c} the observed positive isotropic shifts of the *m*-tolyl carbons in positions 5,15 must be the consequence of a contribution of $+26$ ppm (**2**) or $+10$ ppm (**1**) from the corrolate radical. The same contribution to substituents at position 10 is around 0, leaving isotropic shifts with similar values to that expected merely for the delocalization of the metal electrons. Table 5 also shows the ratio between the ^{13}C and ^1H isotropic shifts. These ratios are expected to be always negative, due to the negative sign of the constant relating the paramagnetic shifts of the two nuclei. As can be seen, this is the sign for all the ratios except for that of the ^{13}C and ^1H nuclei in the meta position of the 10-tolyl group. Once again, this is pointing to a peculiar value of the total spin density at these positions, different from that observed for the other two tolyl groups meta nuclei. This result is in agreement with DFT calculations, which predict a less-pronounced conjugation of the 10-tolyl substituent with the corrole ring.

This behavior can also give some insights into the different reactivity observed for the meso positions of the corrole ring; for example, usually oxidation⁵⁰ and also the oxidative ring-opening³⁴ or corrole ring expansion to give hemiporphycene⁵¹ or azahemiporphycene^{52–54} rings have been always observed to involve the 5-position.

Table 5. ^{13}C Chemical Shifts of Tolyl Substituents in Complexes **1** and **2** in CDCl_3 at 300 K, and the Corresponding Ratios between ^{13}C and ^1H Isotropic Shifts

1			2			assignment
chemical shift ppm	isotropic shift ^a ppm	$^{13}\text{C}/^1\text{H}$	chemical shift ppm	isotropic shift ppm	$^{13}\text{C}/^1\text{H}$	
41.3, 37.4	-93.3, -96.6	-14.1, -16.9	-189.9, -177.9	-324.2, -312.2	-18.4, -19.0	S,15- <i>o</i> -Ph-C
14.4, 11.8	-120.1, -122.0	-30.7, -31.3	-278.9, -265.6	-413.1, -399.4	-26.3, -25.3	10- <i>o</i> -Ph-C
133.9, 132.5	5.4, 4.0	-3.4, -2.1	149.8, 149.4	20.8, 21.2	-2.0, -2.0	S,15- <i>m</i> -Ph-C
124.2, 123.1	-4.0, -5.1	+1.8, +2.1	126.1, 122.6	-5.7, -2.2	+0.5, +0.2	10- <i>m</i> -Ph-C
26.4	5.0	-2.6	51.5	30.1	-2.1	S,15- <i>p</i> -Ph-CH ₃
28.2	6.8	-3.2	46.9	25.5	-2.1	10- <i>p</i> -Ph-CH ₃

^aIsotropic shift = observed chemical shift - diamagnetic shift. Diamagnetic shifts were taken from the corresponding Ge derivatives.

■ ASSOCIATED CONTENT

Supporting Information

CIF file of **1**, structure of the asymmetric unit cell, and ^1H NMR Curie plot of **1**. This material is available free of charge via the Internet at <http://pubs.acs.org>

■ AUTHOR INFORMATION

Corresponding Authors

*E-mail: roberto.paolesse@uniroma2.it. (R.P.)

*E-mail: angela.rosa@unibas.it. (A.R.)

*E-mail: kmsmith@lsu.edu. (K.M.S.)

Notes

The authors declare no competing financial interest.

■ ACKNOWLEDGMENTS

This research was supported by the MIUR (R.P. Grant PRIN 2009 2009Z9ASCA) and U.S. National Institutes of Health (K.M.S. Grant CA 132861). Upgrade of the diffractometer was made possible by Grant No. LEQSF(2011–12)-ENH-TR-01, administered by the Louisiana Board of Regents. A.R. and G.R. thank the Università della Basilicata for financial support (RIL_2011 funds).

■ REFERENCES

- (1) Johnson, A. W.; Kay, I. T. *J. Chem Soc.* **1965**, 1620.
- (2) Paolesse, R. *The Porphyrin Handbook*, Vol. 2; Kadish, K. M., Smith, K. M., Guilard, R., Eds.; Academic Press: New York, 2000; pp 201–232.
- (3) (a) Paolesse, R. *Synlett* **2008**, 2215. (b) Lemon, C. M.; Brothers, P. J. *J. Porphyrins Phthalocyanines* **2011**, *15*, 809. (c) Gross, Z.; Aviv-Harel, I. *Coord. Chem. Rev.* **2011**, *255*, 717–736.
- (4) (a) Gross, Z.; Aviv-Harel, I. *Chem.—Eur. J.* **2009**, *15*, 8382–8394. (b) Barbe, J.-M.; Canard, G.; Brandès, S.; Guilard, R. *Chem.—Eur. J.* **2007**, *13*, 2118. (c) He, C.-L.; Ren, F. L.; Zhang, X.-B.; Han, Z.-X. *Talanta* **2006**, *70*, 364. (d) Gatto, E.; Malik, M. A.; Di Natale, C.; Paolesse, R.; D’Amico, A.; Lundström, I.; Filippini, D. *Chem.—Eur. J.* **2008**, *14*, 6057.
- (5) (a) Cai, S.; Walker, F. A.; Licoccia, S. *Inorg. Chem.* **2000**, *39*, 3466. (b) Nardis, S.; Paolesse, R.; Licoccia, S.; Fronczek, F. R.; Vicente, M. G. H.; Shokhireva, T. K.; Cai, S.; Walker, F. A. *Inorg. Chem.* **2005**, *44*, 7030. (c) Walker, F. A.; Licoccia, S.; Paolesse, R. *J. Inorg. Biochem.* **2006**, *100*, 810. and references therein. (d) Roos, B. O.; Veryazov, V.; Conradi, J.; Taylor, P. R.; Ghosh, A. *J. Phys. Chem. B* **2008**, *112*, 14099. (e) Pierloot, K.; Zhao, H.; Vancoillie, S. *Inorg. Chem.* **2010**, *49*, 10316. (f) Ye, S.; Tuttle, T.; Bill, E.; Simkhovich, L.; Gross, Z.; Thiel, W.; Neese, F. *Chem.—Eur. J.* **2008**, *14*, 10839.
- (6) Licoccia, S.; Paci, M.; Paolesse, R.; Boschi, T. *J. Chem. Soc., Dalton Trans.* **1991**, 461.
- (7) Vogel, E.; Will, S.; Schulze Tilling, A.; Neumann, L.; Lex, J.; Bill, E.; Trautwein, A. X.; Wieghardt, K. *Angew. Chem., Int. Ed.* **1994**, *33*, 731.
- (8) Stefanelli, M.; Nardis, S.; Tortora, L.; Fronczek, F. R.; Smith, K. M.; Licoccia, S.; Paolesse, R. *Chem. Commun.* **2011**, *47*, 4255–4257.
- (9) Nardis, S.; Stefanelli, M.; Mohite, P.; Pomarico, G.; Tortora, L.; Manowong, M.; Chen, P.; Kadish, K. M.; Fronczek, F. R.; McCandless, G. T.; Smith, K. M.; Licoccia, S.; Paolesse, R. *Inorg. Chem.* **2012**, *51*, 3910–3920.
- (10) Evans, D. F. *J. Chem. Soc.* **1959**, 2003.
- (11) Sur, S. K. *J. Magn. Reson.* **1989**, *82*, 169.
- (12) Kahn, O. *Molecular Magnetism*; VCH Publishers: Weinheim, Germany, 1993; pp 2–4.
- (13) Zakharieva, O.; Schünemann, V.; Gerdan, M.; Licoccia, S.; Cai, S.; Walker, F. A.; Trautwein, A. X. *J. Am. Chem. Soc.* **2002**, *124*, 6636.
- (14) (a) ADF2013, SCM, *Theoretical Chemistry*; Vrije Universiteit: Amsterdam, The Netherlands, <http://www.scm.com>; (b) te Velde, G.; Bickelhaupt, F. M.; van Gisbergen, S. J. A.; Fonseca Guerra, C.; Baerends, E. J.; Snijders, J. G.; Ziegler, T. *J. Comput. Chem.* **2001**, *22*, 931. (c) Fonseca Guerra, C.; Snijders, J. G.; te Velde, G.; Snijders, J. G. *Theor. Chem. Acc.* **1998**, *99*, 391.
- (15) Swart, M. *Chem. Phys. Lett.* **2013**, *580*, 166.
- (16) Grimme, S.; Antony, J.; Ehrlich, S.; Krieg, H. *J. Chem. Phys.* **2010**, *132*, 154104.
- (17) Grimme, S. *WIREs Comput. Mol. Sci.* **2011**, *1*, 211.
- (18) Becke, A. D. *J. Chem. Phys.* **1993**, *98*, S648.
- (19) Lee, C.; Yang, W.; Parr, R. G. *Phys. Rev. B* **1988**, *37*, 785.
- (20) van Lenthe, E.; Baerends, E. J.; Snijders, J. G. *J. Chem. Phys.* **1993**, *99*, 4597.
- (21) van Lenthe, E.; Baerends, E. J.; Snijders, J. G. *J. Chem. Phys.* **1994**, *101*, 9783.
- (22) van Lenthe, E.; Ehlers, A. W.; Baerends, E. J. *J. Chem. Phys.* **1999**, *110*, 8543.
- (23) van Lenthe, E.; Baerends, E. J. *J. Comput. Chem.* **2003**, *24*, 1142.
- (24) Klamt, A.; Schürmann, G. *J. Chem. Soc., Perkin Trans.* **1993**, *2*, 799.
- (25) Klamt, A. *J. Phys. Chem.* **1995**, *99*, 2224.
- (26) Pye, C. C.; Ziegler, T. *Theor. Chem. Acc.* **1999**, *101*, 396.
- (27) (a) TURBOMOLE V6.3 2011, a development of University of Karlsruhe and Forschungszentrum Karlsruhe GmbH, 1989–2007, TURBOMOLE GmbH, since 2007; available from <http://www.turbomole.com>. (b) Ahlrichs, R.; Bär, M.; Häser, M.; Horn, H.; Kölmel, C. *Chem. Phys. Lett.* **1989**, *162*, 165.
- (28) (a) Becke, A. D. *Phys. Rev. A* **1988**, *38* (6), 3098. (b) Perdew, J. P. *Phys. Rev. B* **1986**, *33* (12), 8822.
- (29) Weigend, F.; Ahlrichs, R. *Phys. Chem. Chem. Phys.* **2005**, *7*, 3297.
- (30) (a) Laaksonen, L. *J. Mol. Graphics* **1992**, *10*, 33–34. (b) Bergman, D. L.; Laaksonen, L.; Laaksonen, A. *J. Mol. Graphics Modell.* **1997**, *15*, 301.
- (31) Paolesse, R.; Marini, A.; Nardis, S.; Froio, A.; Mandoj, F.; Nurco, D.; Prodi, L.; Montalti, M.; Smith, K. M. *J. Porphyrins Phthalocyanines* **2003**, *7*, 23.
- (32) Nardis, S.; Pomarico, G.; Mandoj, F.; Fronczek, F. R.; Smith, K. M.; Paolesse, R. *J. Porphyrins Phthalocyanines* **2010**, *14*, 752.
- (33) Cai, S.; Licoccia, S.; D’Ottavi, C.; Paolesse, R.; Nardis, S.; Bulach, V.; Zimmer, B.; Shokhireva, T. K.; Walker, F. A. *Inorg. Chim. Acta* **2002**, *339*, 171.

- (34) Nardis, S.; Mandoj, F.; Paolesse, R.; Fronczek, F. R.; Smith, K. M.; Prodi, L.; Montalti, M.; Battistini, G. *Eur. J. Inorg. Chem.* **2007**, 2345.
- (35) Spek, A. L. *Acta Crystallogr., Sect. D: Biol. Crystallogr.* **2009**, 65, 148.
- (36) Van Caemelbecke, E.; Will, S.; Autret, M.; Adamian, V. A.; Lex, J.; Gisselbrecht, J.-P.; Gross, M.; Vogel, E.; Kadish, K. M. *Inorg. Chem.* **1996**, 35, 184.
- (37) Zakharieva, O.; Schünemann, V.; Gerdan, M.; Licoccia, S.; Cai, S.; Walker, A.; Trautwein, A. X. *J. Am. Chem. Soc.* **2002**, 124, 6636–6648.
- (38) Ghosh, A.; Steene, E. *J. Biol. Inorg. Chem.* **2001**, 6, 739.
- (39) Steene, E.; Wondimagegn, T.; Ghosh, A. *J. Phys. Chem. B* **2001**, 105, 11406.
- (40) Ghosh, A.; Steene, E. *J. Inorg. Biochem.* **2002**, 91, 423.
- (41) Walker, F. A. *Inorg. Chem.* **2003**, 42, 4526.
- (42) Rosa, A.; Ricciardi, G.; Baerends, E. J. *J. Phys. Chem. A* **2006**, 110, S180.
- (43) Simkhovich, L.; Galili, N.; Saltsman, I.; Goldberg, I.; Gross, Z. *Inorg. Chem.* **2000**, 39, 2704.
- (44) Rosa, A.; Ricciardi, G. *Inorg. Chem.* **2012**, 51, 9833 and references therein.
- (45) Balch, A. L.; Renner, M. W. *J. Am. Chem. Soc.* **1986**, 108, 2603.
- (46) Simkhovich, L.; Gross, Z. *Inorg. Chem.* **2004**, 43, 6136.
- (47) Bertini, I.; Luchinat, C.; Parigi, G.; Walker, F. A. *J. Biol. Inorg. Chem.* **1999**, 4, 515.
- (48) Goff, H. M. *J. Am. Chem. Soc.* **1981**, 103, 3714.
- (49) Walker, F. A. Chapter 36. In *The Porphyrin Handbook*; Kadish, K. M., Smith, K. M., Guilard, R., Eds.; Academic Press: San Diego, CA, 2000; Vol. 5, p 81.
- (50) Schwalbe, M.; Dogutan, D. K.; Stoian, S. A.; Teets, T. S.; Nocera, D. G. *Inorg. Chem.* **2011**, 50, 1368.
- (51) Paolesse, R.; Nardis, S.; Stefanelli, M.; Fronczek, F. R.; Vicente, M. G. H. *Angew. Chem., Int. Ed.* **2005**, 44, 3047.
- (52) Mandoj, F.; Stefanelli, M.; Nardis, S.; Mastroianni, M.; Fronczek, F. R.; Smith, K. M.; Paolesse, R. *Chem. Commun.* **2009**, 1580.
- (53) Mandoj, F.; Nardis, S.; Pomarico, G.; Stefanelli, M.; Schiaffino, L.; Ercolani, G.; Prodi, L.; Genovese, D.; Zaccheroni, N.; Fronczek, F. R.; Smith, K. M.; Xiao, X.; Shen, J.; Kadish, K. M.; Paolesse, R. *Inorg. Chem.* **2009**, 48, 10346.
- (54) Singh, P.; Dutta, G.; Goldberg, I.; Mahammed, A.; Gross, Z. *Inorg. Chem.* **2013**, 52, 9349.